Rotor/Wake Aerodynamics Assignment 1

Ahmed, Sherif,6281435
Harder, Bjorn, 5070287
Platenburg, Jarno, 5321484

April 2024

1 Introduction

With the ever increasing demand for renewable energy in the energy transition, more and more interest is diverted to wind energy. For this, it is important to know how a wind turbine will perform. The actuator disk theory is method to estimate the performance of a propellor or wind turbine as an one dimensional flow. Its concept is based on momentum. When the rotor of a wind turbine rotates it takes away energy from the flow expanding the control volume and slowing down the air. From this a rough estimation about performance can be made. Although this gives a rough estimation of performance, this is not a accurate enough for modern applications. Blade Element Momentum (BEM) models take this concept and expand it. First the disk is divided into annuli, regions bounded by two concentric circles in a plane. The momentum theory is applied to each annulus' streamtube instead of over the entire disk. Each annulus is assumed to be independent of the other. These annuli are then discretized into azimuthal sections over which the actuator disk theory equations are applied. Both axial and tangential loading are present and each results in their own inductions in the flow. The total of the axial and tangential loading will result in thrust and torque, respectively. The thrust will slow the wake down and the torque will create rotation in the wake. This is also what rotates the blades in the opposite direction and generates power. The blades of the wind turbine are analysed using strip theory with an airfoil in 2D flow for each annulus. Lift and drag forces are calculated using their respecitve coefficients which are specific of the airfoil and the angle of attack. The angle of attack is is dependent on the Tip speed ratio(TSR) wind speed and also on the design angle of the airflow with respect to the rotor plane. The lift and drag forces result in the tangential and normal forces. The momentum theory is then compared with the strip theory results with an initial guess of the axial and azimuthal inductions. This results in loads and velocity at the blade element and from this new inductions can be calculated. This is iterated until the difference between inductions of the previous and the current iteration is small enough. Now the performance of the wind turbine can be estimated with a more accurate estimate than with just the actuator disk theory. In this paper we have programmed a BEM model for a wind turbine with the specifications in Table 1 in $10\frac{m}{s}$ wind for three different TSR's.

Table 1: Rotor Specifications

Parameter	**Value**
Rotor Radius (R)	50 m
Number of Blades (B)	3
Blade Start (r/R)	0.2
Twist (β)	$14(1 - r/R)$ degrees (for $r/R > 0.2$)
Blade Pitch (θ)	-2 degrees
Chord Distribution ($c(r)$)	$3(1 - r/R) + 1$ m (for $r/R > 0.2$)
Airfoil	DU 95-W-180

2 Flow Chart

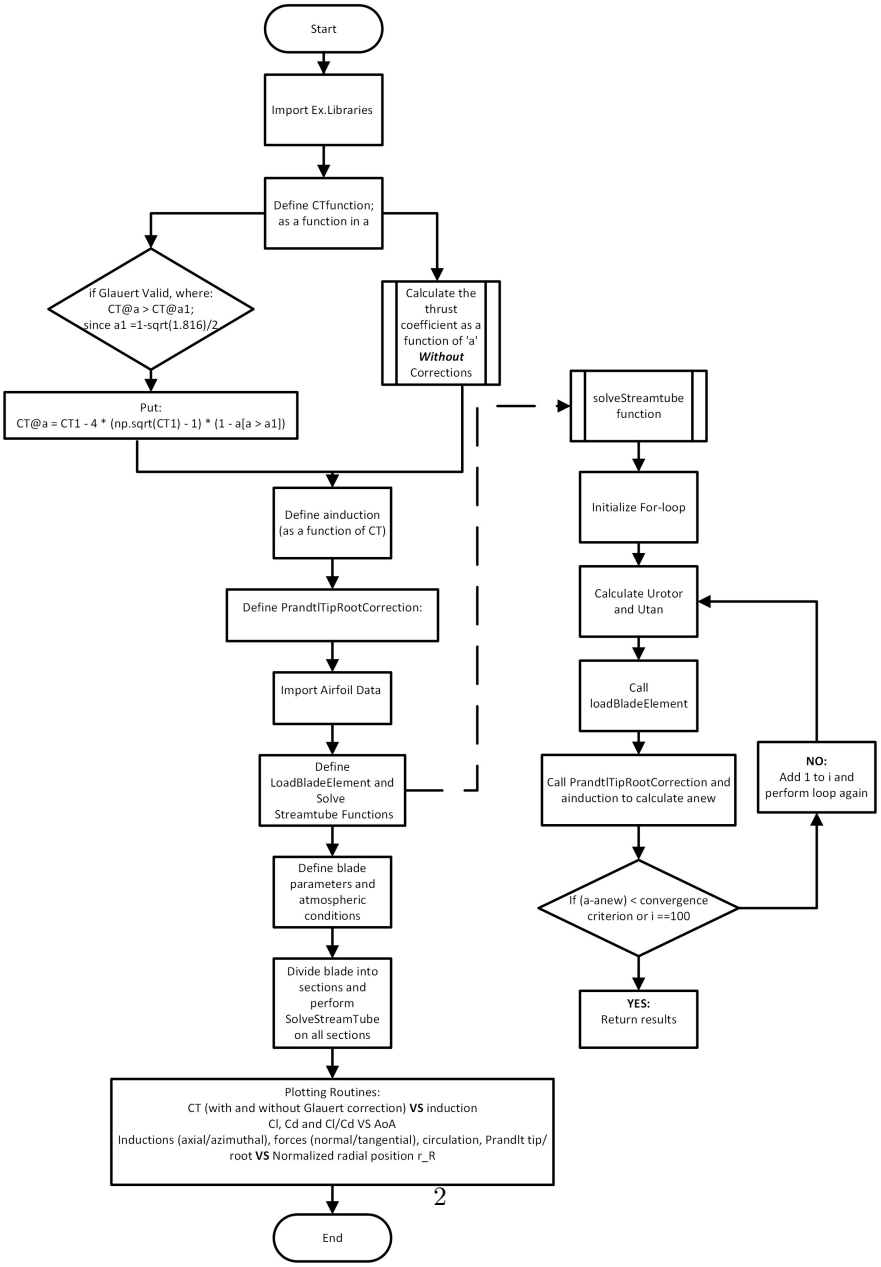

Figure 1: Flow Chart of the code

The flowchart in Figure 1 represents a structured approach to analyze and visualize various aspects of wind turbine performance, facilitating insights into aerodynamic behaviour, correction factors, and overall power generation capabilities. The associated Python code implements these analyses and visualizations, enabling us to assess and optimize wind turbine designs effectively. It should be noted that this flowchart represents the code as if the program solves for only one Tip-Speed Ratio. However, in the enclosed code, an additional loop is added to perform the calculations for multiple Tip-Speed Ratio's. This was omitted from the flowchart as this part is optional, depending on what the user wants.

3 Assumptions

For this assignment assumptions are made. Firstly, steady state conditions are assumed. The flow is fully developed and there are no fluctuations in the incoming wind speed. The wind flows without yaw misalignment and wind direction does not change. In reality, the incoming wind speed and direction fluctuates over time. Secondly, no vorticity and viscosity is present in the airflow which would be there in real life. Thirdly, it is assumed that the blades are rigid. In reality, due to aeroelastic deformation, there will be a difference in twist. Taking this into account can would significantly complicate the calculations since calculating the aeroelastic effects is also an iterative process. Additionally, the flow is assumed to be uniform. Just as in time the flow speed would in real life fluctuate in space due to turbulence, differences in surface roughness and the atmospheric boundary layer. Each BEM section is also treated independently, whereas the flow in over a real turbine blade section is influenced by the sections adjacent to it. Lastly, each section has a single discreet angle of attack value, whereas it is a continuous transition in angle of attack from blade tip to base in reality. All these assumptions are made to enhance the computational process and these factors can be neglected when predicting wind turbine performance.

4 Results

4.1 Spanwise distribution of angle of attack and inflow angle

Figure 2 shows both the inflow angle and the angle of attack spanwise distributed for different tip speed ratios(TSR). When te TSR increases both the inflow angle and the angle of attack decreases. This is as expected since the tangential component of both increases. Since the part of the blade moves faster the closer you get to the edge, you see the angle of attack and inflow angle decrease when increasing r/R.

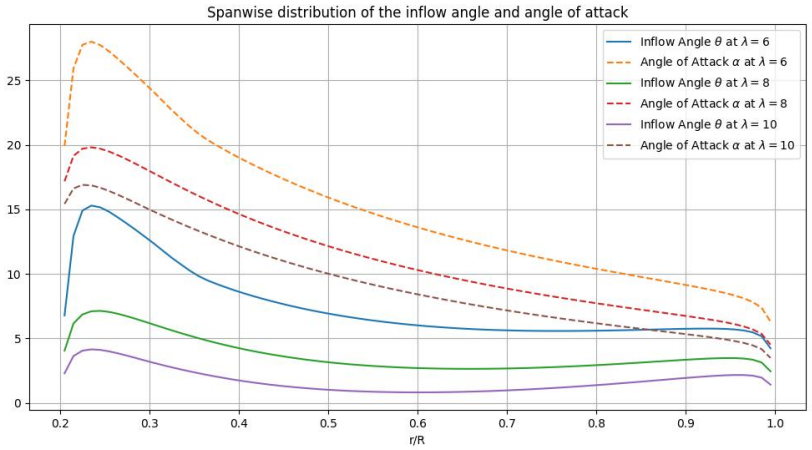

Figure 2: Spanwise distribution of aerodynamic angles for multiple Tip-Speed Ratio's

4.2 Spanwise distribution of axial and azimuthal inductions

Figure 3 illustrates the axial and tangential induction distributions along the blade span (r/R) for different Tip Speed Ratios (TSR) of 6, 8, and 10. The plot demonstrates how these induction factors vary with radial position and under varying operational conditions. Interestingly, the changes in TSR do not exhibit a substantial impact on the induction factors. Despite the variations in TSR values, the trends in axial and tangential induction remain relatively consistent across different TSR values. This observation suggests that the operational efficiency of the wind turbine may not be significantly influenced by variations in TSR within the range examined in this analysis. Further investigation into the underlying aerodynamic mechanisms governing induction factor variations could provide valuable insights into turbine performance under different operating conditions.

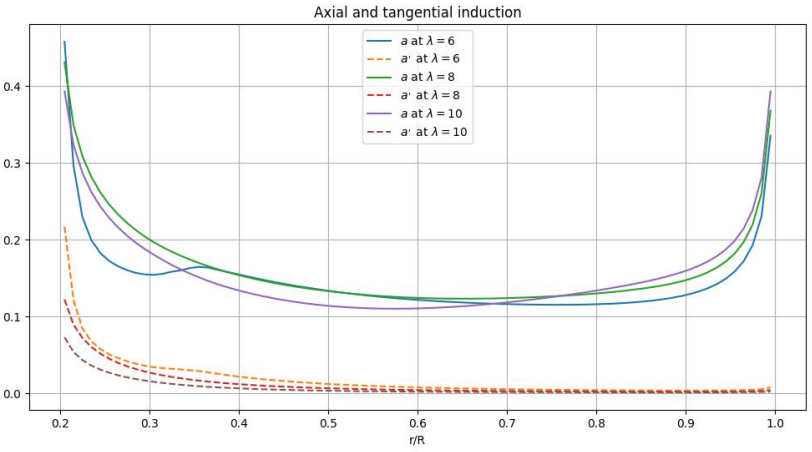

Figure 3: Spanwise distribution of axial and tangential inductions for multiple Tip-Speed Ratio's

4.3 Spanwise distribution of thrust and azimuthal loading

Figure 4 visualizes the distribution of normal and tangential forces exerted on the blade elements along the span (r/R) for different tip-speed ratios (TSR). It offers a comprehensive understanding of how aerodynamic forces evolve with radial position and under varying operational conditions. Particularly noteworthy is the strong impact observed on the normal force close to the tip (approximately 0.7 of the span). This observation underscores the significance of considering the distribution of forces across the blade span when analyzing wind turbine performance and blade structure design (maybe this is why chord length is way shorter than at the root).

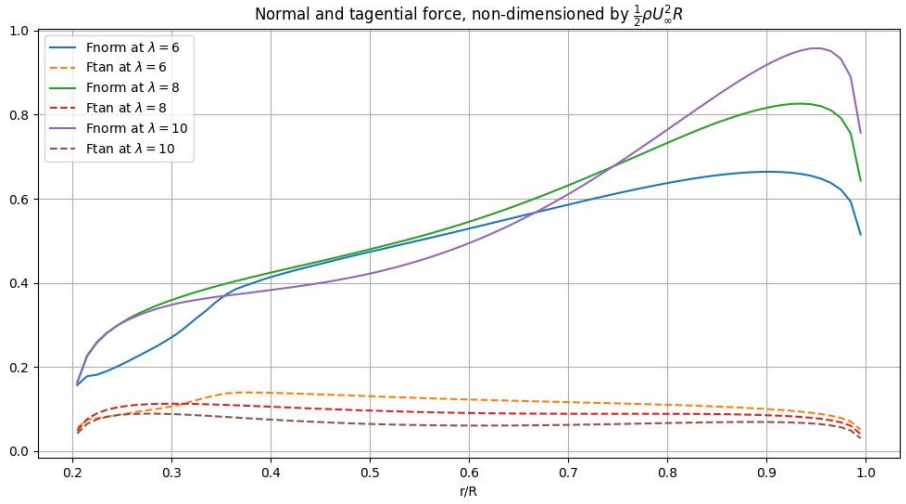

Figure 4: Spanwise force distribution for multiple Tip-Speed Ratio's

4.4 Total thrust and torque vs TSR

Figure 5 demonstrates how the total thrust from the wind turbine changes with different Tip-Speed Ratios (TSRs). As TSR increases, thrust also rises, but the rate of increase slows down at higher TSR values. This implies that while raising TSR can boost thrust, there are diminishing returns beyond a certain point. The curve peaks at an optimal TSR of 9, beyond which thrust gradually decreases. This trend reflects the wind turbine's aerodynamic behavior: increasing TSR initially enhances energy capture until it reaches an optimal point (TSR 9), after which further increases lead to aerodynamic losses and reduced thrust.

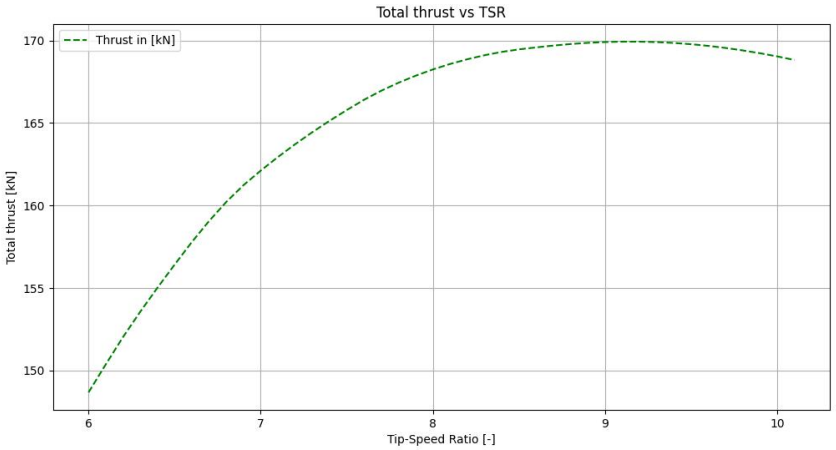

Figure 5: Total thrust vs TSR

Figure 6 demonstrates as TSR increases, the total torque decreases almost linearly, indicating a reduction in the rotational force generated by the turbine. This observation suggests that higher TSR values lead to a decrease in torque efficiency. However, Figure 7 shows after expanding the range of TSR and making it from 1-10, the torque shows a linear increase from TSR 2 till optimum value at TSR around 5 then returns to decrease again. While the linear decrease in torque with increasing TSR (From 6 to 10) can be attributed to aerodynamic effects like stall, the initial increase followed by a decline indicates optimal operating conditions within the turbine's design constraints.

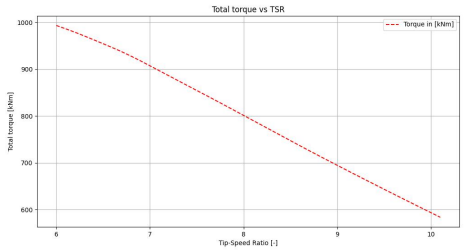

Figure 6: Total torque vs TSR (From 6-10)

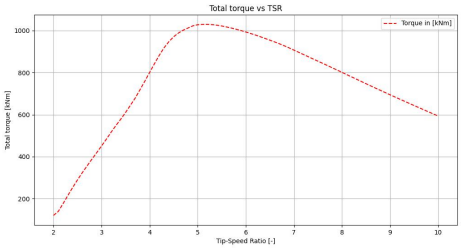

Figure 7: Total torque vs wider range of TSR (1-10)

4.5 Analysis of the Prandtl and Glauert corrections

Figure 8 shows the analysis of wind turbine performance, particularly focusing on the thrust and power coefficients (CT and CP), provides valuable insights into the efficiency and behaviour of wind turbines under varying conditions. By using Glauert's correction, we can refine our understanding of these coefficients, especially in scenarios involving heavily loaded rotors. The Glauert's correction is applied when 'a' exceeds the correction threshold criterion, and adjusts the calculated CT values for conditions where the rotor operates at high thrust coefficients, leading to a more accurate representation of turbine performance. The graph indicates the beginning

of Glauert's correction and highlights the affected area. It also identifies the optimal CP point, representing maximum power extraction efficiency, marked at (0.59).

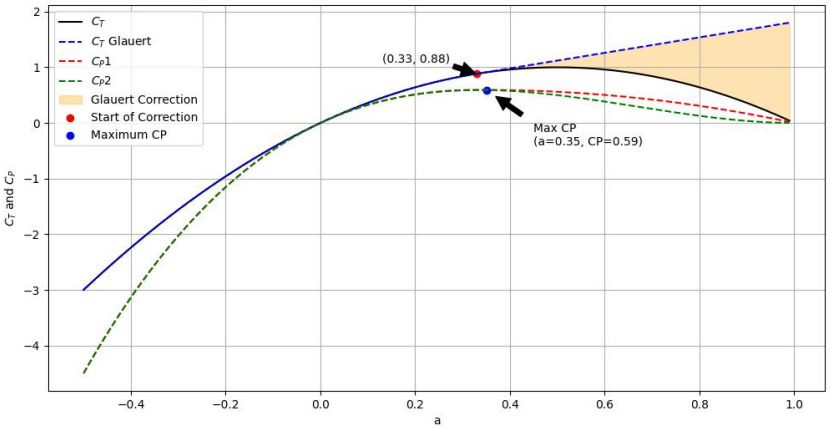

Figure 8: Glauert Correction

By considering different parameters such as the number of blades and axial induction factors, the analysis provides objective insights into the aerodynamic characteristics of the rotor. These findings contribute to enhancing our understanding of wind turbine performance and support the optimization of wind energy systems. Figure 9; illustrates the Prandtl tip, root, and combined correction factors over the non-dimensional radius of the wind turbine blade. The highlighted zone represents the optimum zone, where the maximum energy extraction can be gained.

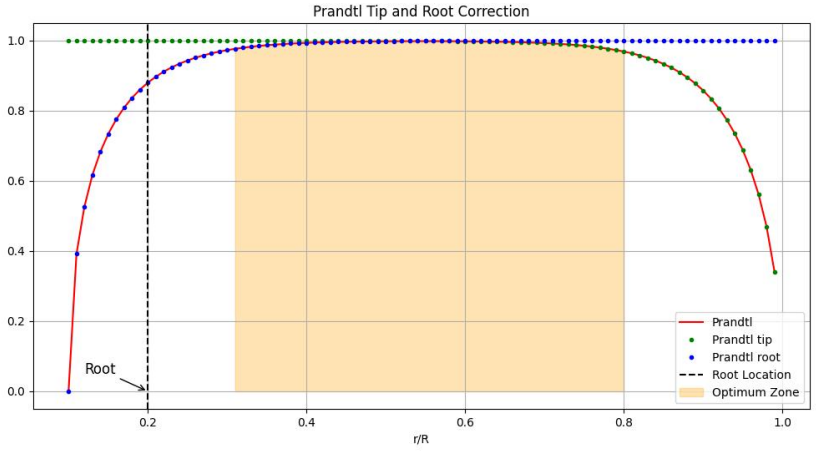

Figure 9: Prandtl Correction

4.6 Distribution of stagnation pressure as a function of radius

In this section, the distribution of the stagnation pressure as a function of the blade radius will be analyzed. It is evaluated at four different locations: Infinitely far upstream, upstream of the rotor, downstream of the rotor and infinitely far downstream. However, both upstream locations and downstream locations will have the same stagnation pressure. It is known that the stagnation pressure can change in space as a consequence of four effects, namely:

1. Acceleration of a flow field
2. External forces applied to the flow
3. Presence of a vorticity field
4. Viscosity effects

In this steady, inviscid flow without vorticiy, as mentioned in the assumptions, there is no presence of effects 1, 3 and 4. However, there is a presence of a force field which is only located at the rotor. The only change in stagnation pressure will thus be made when the flow passes through the rotor. Upstream and downstream of the rotor, it stays constant.

Figure 10 shows the upstream and downstream stagnation pressure as a function of the blade radius for four different tip-speed ratio's. Upstream, the tip-speed ratio has no effect on the flow as it has not yet experienced the effects of the force field. When the flow passes through the rotor, its stagnation pressure goes down. The rotor exerts a force in the opposite direction of the flow. The momentum equation, $(p_2 - p_3)A_R = -F_{rw}$, dictates that there will be a negative jump in pressure to conserve momentum. This explains the lower stagnation pressure downstream.

A bigger force means a bigger stagnation pressure jump. The normal force plots in Figure 4 showed that higher tip-speed ratio's will cause higher normal forces towards the tip but a reduction in force towards the root. This explains the lower stagnation pressure at the tips for a higher λ but not near the root.

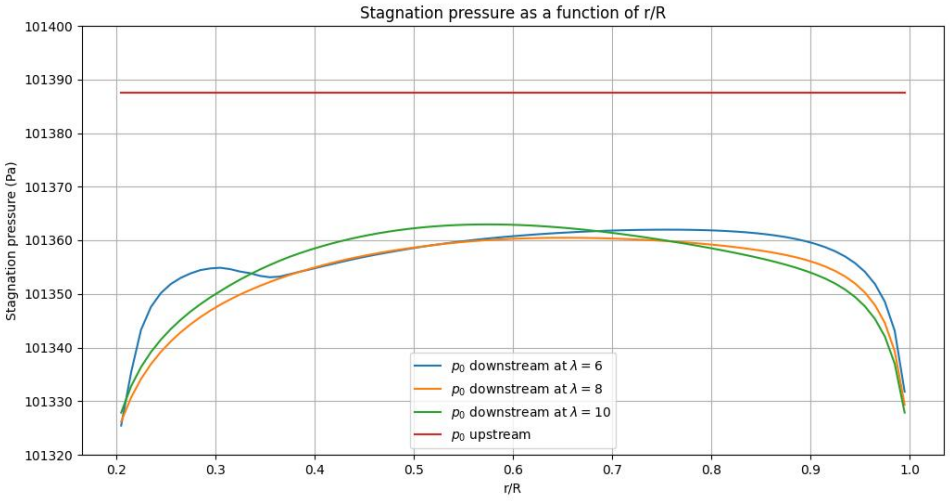

Figure 10: Spanwise distribution of stagnation pressure for multiple Tip-Speed Ratio's

4.7 Operational point of the airfoil

In this analysis, we explored the aerodynamic performance of an airfoil by examining the relationships between Angle of Attack (α), lift coefficient (C_l), drag coefficient (C_d), and their ratio ($\frac{C_l}{C_d}$). By plotting these parameters against α in figure 11, we gained insights into the airfoil's behavior across different operating conditions (AoA). The most informative plot is the third plot. the $\frac{C_l}{C_d}$ vs α, as it depicted the airfoil's efficiency in terms of lift-to-drag ratio. This plot allowed us to identify the optimum operating point where the airfoil achieves the highest lift-to-drag ratio, indicating the most efficient configuration for a given angle of attack. Highlighting the optimum point emphasized the critical operating condition where the airfoil exhibits its best performance. This is at an angle of attack of $\alpha = 8.734°$

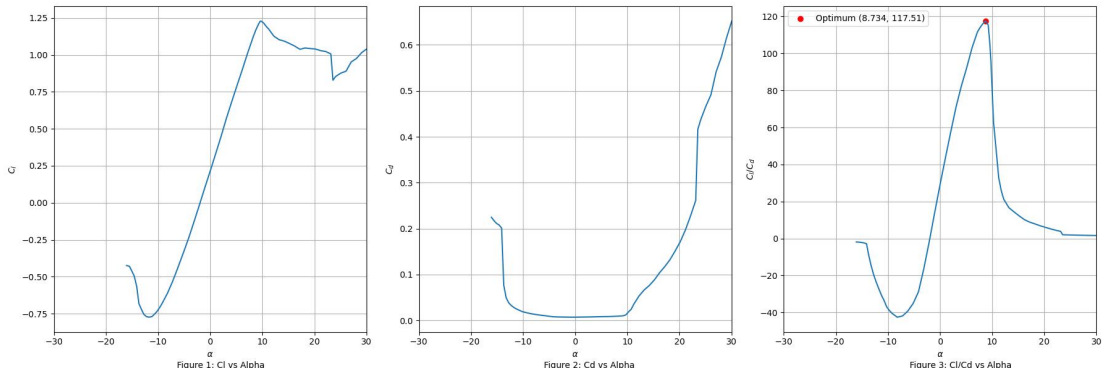

Figure 11: Lift coefficient, Drag coefficient and $\frac{C_l}{C_d}$ plotted against α

5 Conclusion

These results are dependent on the operational specifications. As seen in the graphs, the TSR has an impact on the performance of the turbine. The inflow angle and the angle of attack decrease with increasing TSR, but the induction factors don't massively differ with TSR. The total thrust with respect to TSR peaks at a TSR of 9 and the torque peaks at a TSR of 5. The TSR also influences where the forces are located on the blade and the distribution of the stagnation pressures span wise. The in flowing wind speed of $10\frac{m}{s}$ also influences performance. Until rated wind speed an increase of wind speed would constitute to an increase of performance and decrease of wind speed consequently to an decrease of performance. The wind speed would also influence the optimal TSR and the other results but this is not within the scope of this paper. Most of the assumptions simplify the flow around the turbine. Because of the fluctuations of the real wind this BEM model can be seen as the performance of the wind turbine in the ideal case. In real life the performance will be lower as a result. All these will not change the predicted peak at which TSR, alpha and so forth. The wind turbine will behave the same only at a lower performance than predicted. Only the aeroelastic assumption has an impact on these factors. Since it will change the operating angle of attack in real life. This assumption needs to be compensated to find the real optimum.